

Article

Tailorable Formation of Hierarchical Structure Silica (HMS) and Its Application in Hydrogen Production

Luming Li ^{1,2,3,4}, Jie Deng ^{1,4}, Zhanglong Guo ^{2,4}, Wei Chu ^{4,*} and Yan Liu ^{2,*}¹ School of Food and Biological Engineering, Chengdu University, Chengdu 610106, China² Institute of Sustainability for Chemicals, Energy and Environment, A*STAR, Singapore 627833, Singapore³ Institute for Advanced Study, Chengdu University, Chengdu 610106, China⁴ Department of Chemical Engineering, Sichuan University, Chengdu 610065, China

* Correspondence: chuwei1965@scu.edu.cn (W.C.); liu_yan@isce2.a-star.edu.sg (Y.L.)

Abstract: Relentless endeavors have been committed to seeking simple structure-directing agents for synthesizing hierarchical mesoporous silica (HMS) materials but remaining challenges. In this contribution, we offered an improved one-pot hydrothermal route to prepare HMS materials using a single non-ionic triblock copolymer (F127) structure-directing agent under a mild polycarboxylic (citric acid) mediated condition. Via studies of key synthetic parameters including acid concentration, crystallization temperature and aging time, it was found that citric acid medium presents an important bridging effect under the optimal concentration from 0.018 M (pH = 2.57) to 1.82 M (pH = 1.09), contributing to the self-assemblage of partially protonated non-ionic triblock copolymer and tetraethyl orthosilicate (TEOS) into a high-quality multistage structure of silica materials. The specific surface area (SSA) of HMS shows a volcanic trend and is closely associated with the concentration of citric acid while the highest SSA of 739.9 m²/g can be achieved at the citric concentration of 0.28 M. Moreover, the as-synthesized HMS-CTA supported Ni/CeO₂ catalysts indicate an excellent production of hydrogen through dry reforming of methane (DRM) reaction over 172 h stability. The improved, facile synthesis strategy under polycarboxylic medium displays an expanded perspective for synthesizing other mesoporous materials in a wide range of applications such as catalytic material carriers and drug inhibitors.

Keywords: hierarchical silica; polycarboxylic; protonation; triblock copolymer; catalytic support; hydrogen



Citation: Li, L.; Deng, J.; Guo, Z.; Chu, W.; Liu, Y. Tailorable Formation of Hierarchical Structure Silica (HMS) and Its Application in Hydrogen Production. *Catalysts* **2022**, *12*, 1061. <https://doi.org/10.3390/catal12091061>

Academic Editors: Bing Zhang and Chuntian Qiu

Received: 24 August 2022

Accepted: 15 September 2022

Published: 17 September 2022

Publisher's Note: MDPI stays neutral with regard to jurisdictional claims in published maps and institutional affiliations.



Copyright: © 2022 by the authors. Licensee MDPI, Basel, Switzerland. This article is an open access article distributed under the terms and conditions of the Creative Commons Attribution (CC BY) license (<https://creativecommons.org/licenses/by/4.0/>).

1. Introduction

Hierarchical mesoporous silica (HMS) materials are prestigious porous materials. Their interconnected periodic substructure, high specific surface area as well as high loading capacity are particularly attractive to the wide applications including catalysis, adsorption, separation, life science, and energy storage [1–5]. The most common synthesis route to HMS is implemented via the combinative self-assembly of nonionic block copolymers and silicate molecules [6,7]. For instance, ABC (i.e., PE-b-PEO-b-PCL) and ABA (i.e., PEO-a-PPO-b-PEO-a) type triblock copolymers have attracted great attention owing to their biodegradability, nontoxicity, and excellent interfacial stability. They have been widely applied as structure-directing agents to induce the formation of abundant spatial structure with various morphology (nanoparticles, fibers, and rods), such as cubic mesophase and hexagonal mesophase [8–10].

Generally, the secondary surfactants or additives are always engaged to construct these hierarchical mesoporous silica (HMS) materials [11]. Esquena et al. reported that silica materials characterized with a dual pore size distribution was prepared under highly concentrated co-templating emulsions conditions, where the co-templates consist of emulsion droplets (C₁₂(EO)₈/decane) and cubic liquid crystal of PEO-PPO-PEO block copolymer non-ionic surfactant. The emulsion droplets would induce the formation of macropores whereas

nonionic surfactant would template the formation of the mesopore structure [12]. Zhou et al. synthesized a series of micro/mesoporous silica materials using non-ionic block copolymer Pluronic (P123) and triethylamine acetate (PIL) as co-templates. The sub-structure of silica was closely related to the content of PIL and hydrothermal conditions [13]. Liu et al. prepared hierarchical mesoporous silicas using the triblock copolymer PEO₁₀₆-PPO₇₀-PEO₁₀₆ (F127) and the diblock copolymer poly (ethylene oxide-*b*- ϵ -caprolactone) (PEO-*b*-PCL) as co-templates [14]. Moreover, Shi et al. found that hierarchically porous materials can be obtained from the polyelectrolyte-surfactant complex templating strategy [9]. The combination between surfactant templates and hard templates is another important approach in the formation of the hierarchical pore structure, as Stein et al. reviewed [15]. However, the secondary template would undoubtedly increase the complexity of preparation process, i.e., reaction conditions and formation mechanisms. Therefore, it is urgent to develop an efficient process to prepare hierarchical silica materials using only one type of surfactant to better meet the practical convenience.

Zhao et al. firstly reported that ABC amphiphilic triblock copolymer of poly(ethylene oxide)-block-poly(methyl methacrylate)-block-polystyrene (PEO-*b*-PMMA-*b*-PS) was of great importance for fabricating mesoporous materials [16]. However, the interconnected hydrophobic parts (PMMA and PS) were only capable to induce single hydrophobic domain and produce the mesoporous material with single pore size. Li et al. found that the hierarchical mesoporous silicas featured with two kinds of mesoporous size were synthesized using different hydrophobic segments (poly ethylene and poly ϵ -caprolactone), separately grafted at the chain end of the poly ethylene oxide [17]. It can be concluded that the location of hydrophobic segments plays an important role in strategically forming the hierarchical mesoporous morphology. These two kinds of hydrophobic groups were separately located at the end of the PEO, which showed an advantage in regulating the multistage spatial structure. However, it is rarely reported that these hierarchical silica structures can be prepared using only one ABA type of structure-directing agent (ABA, where the same hydrophobic groups are separately located at the end of the PEO) via a convenient evaporation-induced self-assembly (EISA) strategy [10]. In our previous study, we reported that polycarboxylic acids (citric acid) plays a key role in preparing high-quality mesoporous silica without the addition of mineral acid (HCl) [18]. In this contribution, we deeply investigate the interaction between the non-ionic triblock copolymer and polycarboxylic acid and their influence on the pore structure formation of silica materials. Surprisingly, hierarchical mesoporous silica (HMS) was formed with tunable dual pore structure. Via detailed characterization, we believe that the self-assembly of partially protonated non-ionic triblock copolymer and tetraethyl orthosilicate (TEOS) plays a key role for the formation of high-quality multistage structure of silica materials.

Moreover, the hydrogen economy boom has drawn great attention because of the environmental and energy crisis [19–22] as well as the hydrogenation reaction [23]. Until now, hydrogen can be divided into three categories in view of the process of hydrogen production, namely green hydrogen (preparation hydrogen from renewable energy), purple hydrogen (preparation hydrogen from nuclear energy) and blue hydrogen (preparation hydrogen from coal gasification, natural gas and other derivatives of carbon) [24,25]. The route of hydrogen production via dry reforming of methane (DRM) reaction has become a hot scientific topic, covering the research on active compositions, catalysts carriers as well as their additives [26]. Catalyst support, as one of the core components, is vital to command the interaction strength between the metal and support, dispersion of the active species and the exposure of active center [27]. Undoubtedly, the mesoporous silica is propitious due to its large specific surface area, thermal stability and easy availability [27]. However, the weak interaction between active species and silica carrier causes the sintering of large metal nanoparticles, and formation of carbon deposition, resulting in less formation of hydrogen, especially on Ni-based catalysts [28]. It is usually advocated that the introduction of promoter favors the adjustment of the above drawbacks. For example, the CeO₂ could not only improve the dispersion of Ni nanoparticles, but also activate carbon dioxide

into mobile oxygen species and promote the carbon removal owing to its unique redox properties (), thermal resistance and enhancement of the metal-support interaction [29,30]. In our recent study, we found that the ceria loading interval ranges from 10 wt% to 30 wt% exhibited outstanding production of hydrogen with different carbon deposition resistance. The optimized ceria loading of 15 wt% (5Ni/15CeO₂-SBA-15-CTA) catalyst yielded the best anti-coke performance with the lowest coke deposition rate of 13.5 wt% during 170 h DRM reaction [31]. These above interesting scientific phenomena inspire us to develop novel HMS and to support Ni/CeO₂ catalysts for hydrogen formation via DRM strategy.

2. Results and Discussions

2.1. Formation Mechanism of HMS Materials

Figure 1 depicted that hierarchical mesoporous silica was synthesized using F127 as template under various citric acid concentrations from zero to 0.018 mol/L (pH = 2.57) and 1.82 mol/L (pH = 1.09). Without citric acid, the silica indicates the typical nitrogen adsorption–desorption behavior as mesoporous material [32]. While citric acid was added from 0.18 to 1.03 mol/L, their typical type-IV curves clearly highlights two overlapping hysteresis loops, indicating a hierarchical feature with two types of pores (Figure 1a). Figure 1b presented the pore size distribution curves of the prepared products, the adjustment of mesoporous size hinges on the concentration of citric acid (or pH). The high concentration (i.e., 1.82 mol/L) of acid or low pH would only cause a single mesoporous structure. On the contrary, the relatively low concentration of citric acid would facilitate the synthesis of HMS materials. Results suggest a controllable synthesis of silica materials with double mesoporous structure using a facile approach. Moreover, the specific surface area (SSA) of HMS was also closely associated with the concentration of citric acid. As displayed in Table 1, the SSA showed a volcanic trend with citric concentration for the HMS materials. The highest SSA of 739.9 m²/g (Entry 4) was achieved at the citric concentration of 0.28 mol/L. However, an even higher SSA can be obtained for a single mesoporous silica material at a high concentration of polycarboxylic acid at 1.82 mol/L, which is likely originated from the degree of well-ordered substructure.

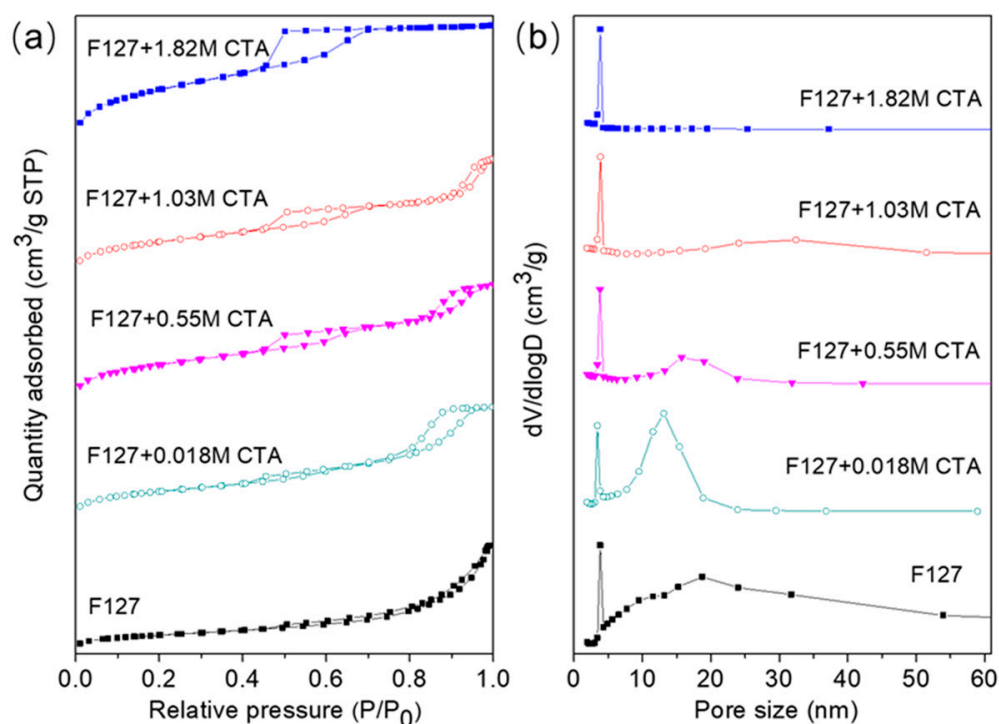
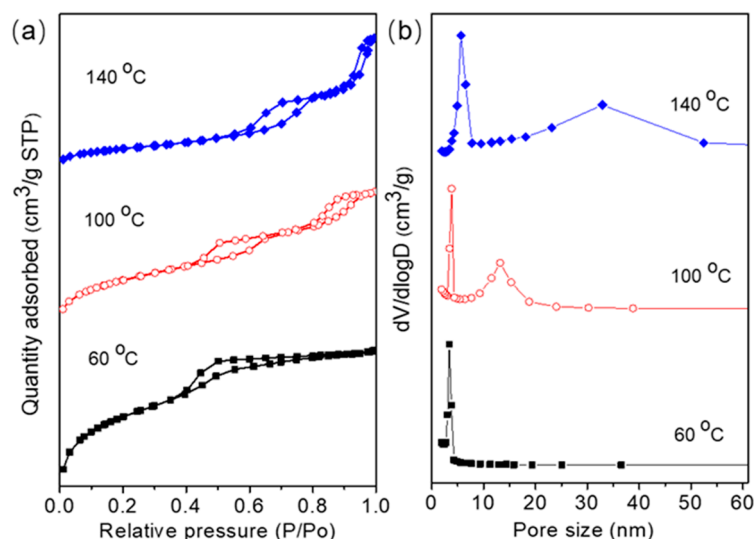


Figure 1. Nitrogen adsorption–desorption isotherms (a) and pore size distribution (b) profiles of the calcined HMS samples.

Table 1. Preparation conditions and physicochemical properties of the synthesized hierarchical mesoporous silica.

| Entry No. | F127 Mass (g) | Citric Concentration (mol/L) | Hydrothermal Temp./Time (°C, h) | pH Value | S_{BET} (m^2/g) | Micropore Area (m^2/g) | Volume (cm^3/g) | Pore Size (nm) |
|-----------|---------------|------------------------------|---------------------------------|----------|--|--|-----------------------------------|----------------|
| 1 | 2.5 | 0 | 100, 24 | 6.80 | 332.9 | 29.3 | 0.78 | 10.84 |
| 2 | 2.5 | 0.018 | 100, 24 | 2.57 | 651.1 | 88.8 | 0.95 | 6.80 |
| 3 | 2.5 | 0.055 | 100, 24 | 2.20 | 690.4 | 86.9 | 0.99 | 6.87 |
| 4 | 2.5 | 0.28 | 100, 24 | 1.82 | 739.9 | 86.4 | 0.75 | 4.78 |
| 5 | 2.5 | 0.55 | 100, 24 | 1.63 | 725.8 | 69.6 | 0.78 | 5.21 |
| 6 | 2.5 | 1.03 | 100, 24 | 1.40 | 703.2 | 74.2 | 0.88 | 5.76 |
| 7 | 2.5 | 1.82 | 100, 24 | 1.09 | 782.4 | 142.7 | 0.61 | 3.45 |
| 8 | 2.5 | 0.28 | 60, 24 | 1.82 | 443.2 | 181.6 | 0.29 | 3.18 |
| 9 | 2.5 | 0.28 | 140, 24 | 1.82 | 565.3 | 26.0 | 1.38 | 9.37 |
| 10 | 2.5 | 0.28 | 100, 4 | 1.82 | 502.3 | 167.1 | 0.36 | 3.44 |
| 11 | 2.5 | 0.28 | 100, 8 | 1.82 | 546.2 | 160.2 | 0.46 | 4.12 |
| 12 | 2.5 | 0.28 | 100, 16 | 1.82 | 702.6 | 104.2 | 0.69 | 4.67 |
| 13 | 2.5 | 0.28 | 100, 48 | 1.82 | 792.3 | 30.3 | 0.95 | 5.13 |
| 14 | 2.5 | 0.28 | 100, 72 | 1.82 | 729.7 | 18.2 | 0.96 | 5.39 |
| 15 | 2.5 | 0.28 | 100, 140 | 1.82 | 745.2 | 34.5 | 1.17 | 6.09 |
| 16 | 2.5 | 0.28 | 100, 480 | 1.82 | 629.7 | 55.7 | 1.16 | 8.28 |
| 17 | 0 | 1.03 | 100, 24 | 1.40 | 586.3 | NA | 1.23 | 7.65 |

It is well known in the literature that the hydrothermal temperature favors adjusting the pore substructure owing to the temperature sensitivity of polymerization between inorganic silicate and copolymer micelle [18,33]. By considering the hydrothermal temperature, a suitable temperature at 100 °C was found to be necessary for preparing the well-ordered double-porous materials. Either higher or lower hydrothermal temperature can cause fatal defects, resulting in the decrease in SSA (e.g., 60 °C, 443.2 m^2/g , Entry 8; 100 °C, 739.9 m^2/g , Entry 8; 140 °C, 565.3 m^2/g , Entry 9), as Figure 2a,b and Table 1 depict.

**Figure 2.** N_2 -BET (a) and pore size distribution (b) curves of HMS materials (Entry No.4) synthesized under different hydrothermal temperature.

Moreover, the hydrothermal time dependence on mesoporous silica materials prepared under 0.28 mol/L citric acid was performed, as shown in Figure 3. It was found that the hierarchical mesoporous silica with two typical hysteresis loops can only be formed while the duration time of hydrothermal was longer than 8 h (e.g., 16 h and 140 h) (Figure 3a). The hierarchical double pores were gradually formed and solidified during the extension

of the hydrothermal treatment time (4 h–8 h–16 h–140 h–480 h). On the other hand, their pore size was positively increased along with the treatment time (Figure 3b and Table 1). Pore size ranges from 3.44 nm (Entry 10, 4 h) to 6.09 nm (Entry 15, 140 h). The variation trend of specific surface area presents a volcanic shape, peaked at $792.3 \text{ m}^2/\text{g}$ (Entry 13). It may suggest that the extended hydrothermal time ($>48 \text{ h}$) would reduce the specific surface area of HMS materials with an enlarged pore size. Results are consistent with the report using the hyper-protonation of PEO block [33], where a stronger affinity to the silicate (TEOS) than that of the hydrophobic PPO block was found under the enduring reaction time, inducing the deep penetration of PEO chains into the frameworks of silicate micelles, and subsequent pore size expansion after calcination. Notably, the hierarchical merit with $629.7 \text{ m}^2/\text{g}$ SSA can be retained under the extended hydrothermal time of 480 h (20 day), indicating the hierarchical double pore structure is hydrothermally stable even with an excessive prolongation of the hydrothermal time up to 20 days (Figure 3a).

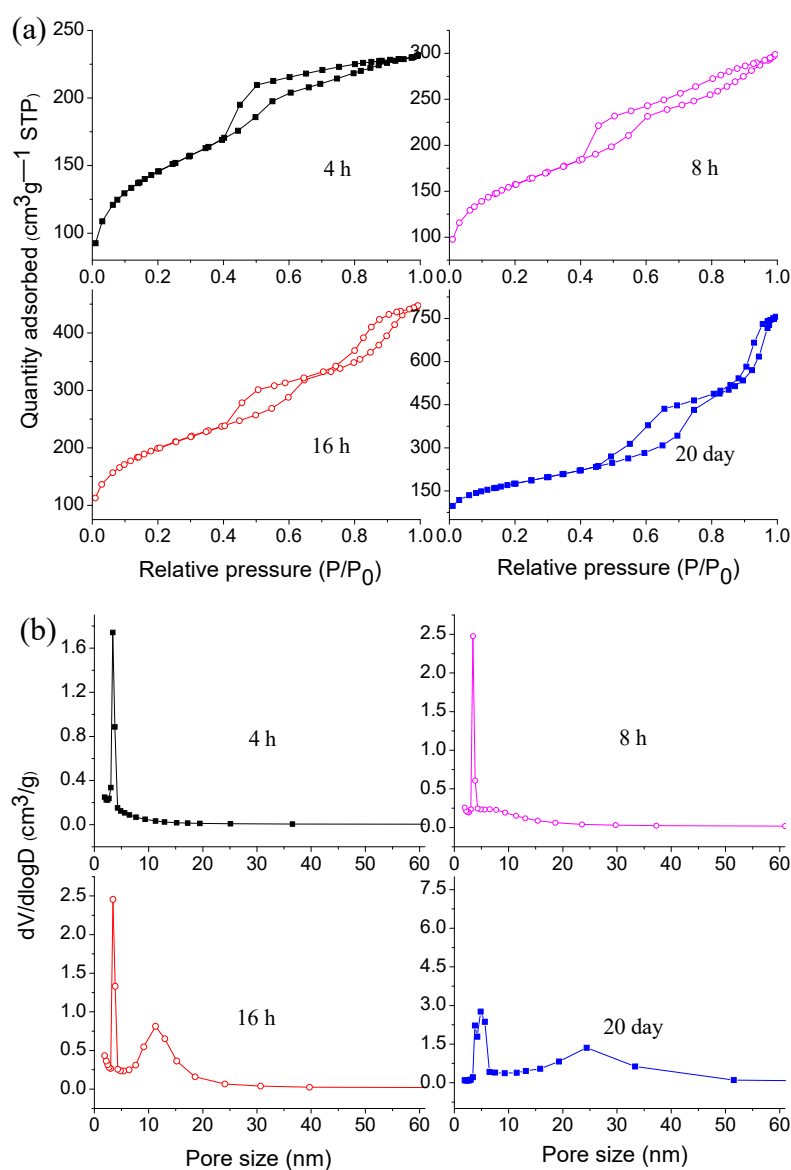


Figure 3. The curves of N_2 -BET (a) and pore size distribution (b) for HMS samples were selected as the function of reaction time ranges from 4 h to 480 h.

From the data of SSA and pore structure, it was inferred that the merit of double-pore structure mainly depends on the mediated dose of citric acid amount and the optimized hydrothermal time ($\geq 16 \text{ h}$). Small-angle ($2\theta = 0\text{--}6^\circ$) XRD patterns were recorded on a

Bruker D8 Advance X-ray diffraction meter, to study the crystal phase or periodic structure of synthesized HMS materials. As shown in Figure 4, no periodic structure was formed only with F127 as surfactants. The mesoporous structure can only be formed with the coordination of F127 and citric acid, clearly indicating the importance of the mediation from citric acid. It was found that the high concentration of citric acid could benefit the formation of well-ordered cubic structure, as the Figure 4 indicated. An apparent diffraction intensity appears with a large d spacing of 115 Å (110), and another two weak diffraction peaks are reflected in the range of 1–1.4° with interplanar d spacing of 72.9 Å (200) and 64.0 Å (211), which should correspond to a cubic structure (*Im3m* space group, SBA-16) [7,34]. Thus, it was worthwhile noting that the silica materials with a periodic pore structure would not be easily synthesized under the low concentration citric modulator.

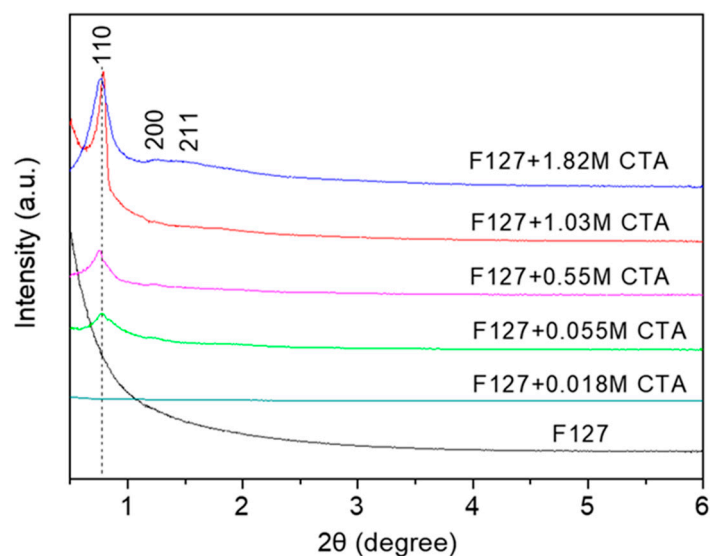


Figure 4. Small-angle XRD patterns of the calcined HMS samples.

In order to uncover the microstructure of the as-prepared HMS materials, we took the measurement of TEM observation of the typical HMS sample synthesized under the CTA concentration of 0.28 mol/L (pH = 1.82) calcined at 550 °C. The TEM and HRTEM (inset) images displayed in Figure 5 exhibit the well-ordered arrays and reveal an anticpant 3D cubic microstructure which corresponds well to the results of small angle XRD and BET measurements.

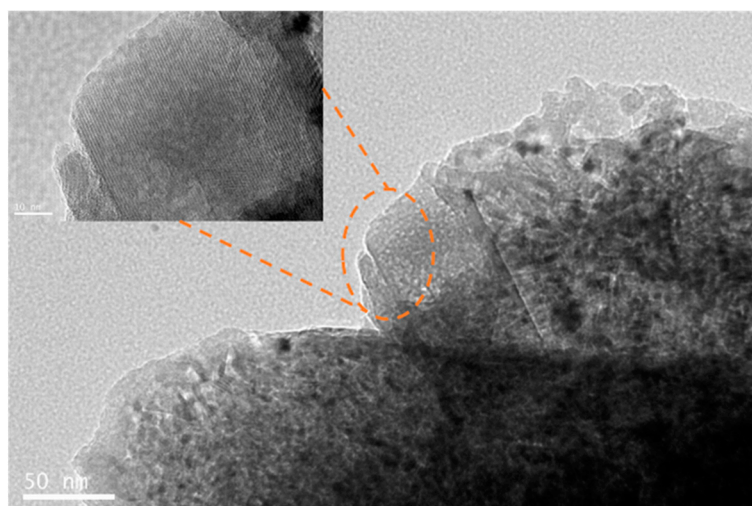
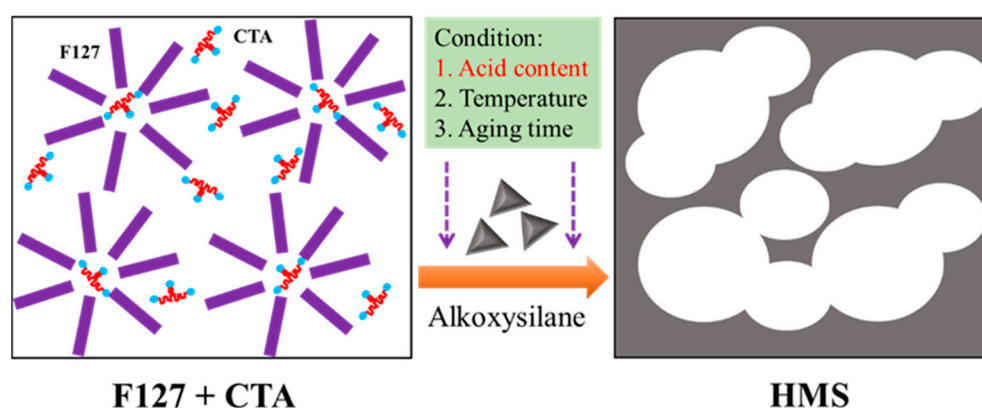


Figure 5. TEM images of HMS calcined at 550 °C.

According to the above characterization results, the microstructure of mesoporous silica is closely related to the synthesis conditions such as concentration of citric acid, hydrothermal temperature as well as hydrothermal time. The proposed formation mechanism was briefly proposed in Scheme 1. Optimal acid conditions (0.018–1.82 mol/L), hydrothermal temperature (100 °C) and hydrothermal time (16 h) were necessary for the synthesis. However, it was noticed that the content of citric regulator is the key controlling parameter to synthesize HMS materials. Stronger acidity (above 1.82 mol/L) would promote a rapid hydrolysis/condensation of silicate species that would form a well-ordered cubic structure (SBA-16). The formation of HMS probably originated from the incomplete condensation of silicate under the mild acid condition (Scheme 1). Moreover, it was accepted that the aging process would enhance the silicate condensation and the hydrothermal stability of the HMS materials. In this contribution, prolonged hydrothermal treatment should not be advocated due to the minor changes in structure, accompanied by the enlargement of the pore size.



Scheme 1. Formation mechanism of an inorganic network of HMS with different pore sizes by applying single non-ionic triblock copolymer (F127) under citric acid condition.

2.2. Catalytic Activity of Ni Based Catalysts in DRM Reaction

These porous silica materials possess high surface areas and tunable pore dimensions (2–50 nm), where the relatively large pores would enhance mass transfer, while the high surface area facilitates the exposure of active centers per mass of catalysts, which are great catalyst carrier candidates for heterogeneous catalysis, such as DRM [27,35,36]. In our previous contributions, high-quality SBA-15-CTA (CTA signifies citric acid) materials with typical 2D hexagonal pore structure have been successfully prepared under moderate polycarboxylic citric acid, being utilized to synthesize Ni/SBA-15-CTA and CeO₂ doped NiCeO₂/SBA-15-CTA hybrid catalysts [18,31]. The catalytic activity results showed that the addition of CeO₂ could significantly improve the sintering resistance properties of Ni and carbon elimination rate due to the strong interaction between Ni nanoparticles and CeO₂ additives [31]. In this contribution, we will secondly explore the relationship between the strong interaction of metal support and its performance on the new hierarchical silica carrier, to evaluate their application prospects of our multi-porous silica materials. Figure 6a displayed the structural periodicity of the synthesized hierarchical materials loaded by the active species of Ni (5 wt%) and additive of CeO₂ (15 wt%); it was found that the addition of active Ni nanoparticles and additive of CeO₂ would not damage the spatial microstructure of HMS materials. However, the SSA of 429.1 m²/g showed a decreasing tendency compared to the SSA of 739.9 m²/g of HMS-CTA parent carrier as the channels are clogged with some nanoparticles (NiO and CeO₂) to some extent (inserted adsorption–desorption curve of Figure 6a). Moreover, the first reduction peak (317 °C) of NiO nanoparticles and surface oxygen in ceria for the 5NiO15CeO₂/HMS-CTA catalyst becomes narrower and shifted to the lower temperature (404 °C, Figure 6b), compared to the 5NiO15CeO₂/SBA-15-CTA (464 °C), revealing that CeO₂ could better promote the

dispersion of NiO nanoparticles on HMS carriers more uniformly compared to that on 2D silica [31,37]. Nevertheless, the second reduction peaks of 404 °C and wide peaks of 450 °C should be attributed to the reduction of NiO species with strong interaction with CeO₂ on HMS support, corresponding well to the previous study [38]. The fourth reduction peak at around 721 °C reflected the reduction of Ce⁴⁺ → Ce³⁺ species [39]. It is worth noting that CeO₂ indeed improves the dispersion of NiO species and strengthens the interaction between metal and carriers of HMS materials.

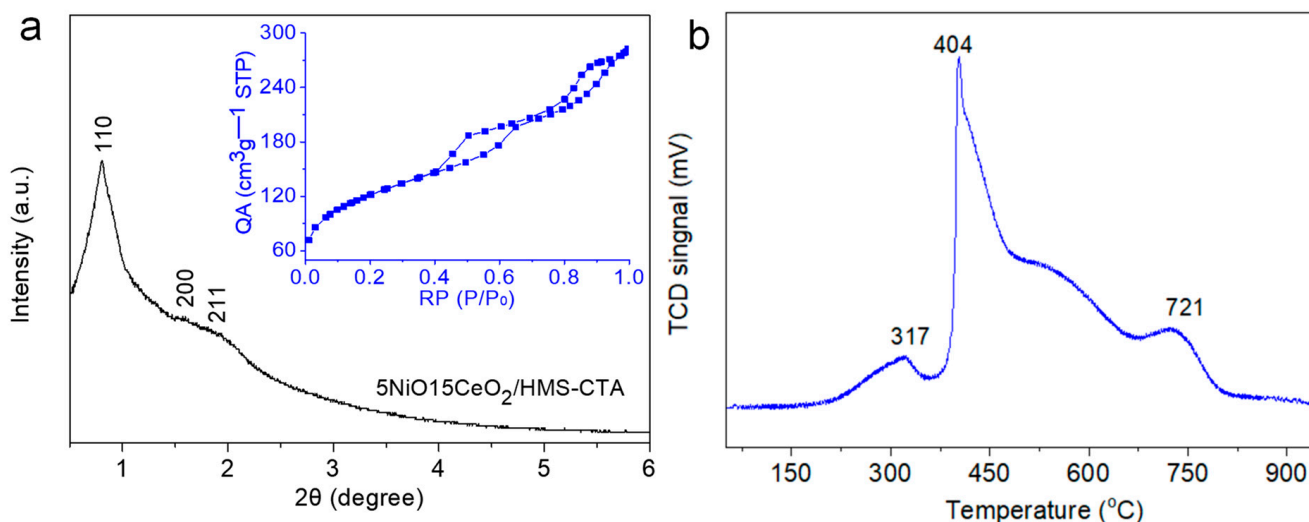


Figure 6. Small-angle XRD pattern (a) of the 5NiO15CeO₂/HMS-CTA catalyst and H₂-TPR (b) profile of 5NiO15CeO₂/HMS-CTA sample, the inserted image (left) correspond to its nitrogen adsorption–desorption isotherms curve.

The catalytic activity of 5NiO15CeO₂/HMS-CTA catalyst was evaluated for 172 h at 700 °C in Figure 7. It was found that the initial conversion of CO₂ and CH₄ reached ca. 77.8% and 73.2%, with 93.2% H₂ selectivity and H₂/CO molar ratio of 0.91. Moreover, CO₂ conversion, CH₄ conversion, H₂ selectivity and H₂/CO molar ratio were maintained at ca. 71.5%, 64.1%, 91.8% and 0.90 after 172 h long term stability testing (Figure 7). The syngas production rate is substantially higher than that of reports on common amorphous silica supported Ni-based catalysts (<85%) [28,30]. Moreover, the weight loss curve on the spent 5NiO15CeO₂/HMS-CTA catalyst was 26.2 wt% for 172 h with a DTA peak of 609 °C (right inserted image in Figure 7), probably further confirming that the graphitic carbon was successfully hindered and the formed coke was more reactive over the 5NiO15CeO₂/HMS-CTA catalyst [40]. Hence, the synthesized HMS materials present a great potential in the heterogeneous catalysis field. In addition, it is noted that the CO₂ conversion was slightly superior to that of CH₄, which is mainly originated from the presence of side effects from reverse water gas shift reaction under high temperature conditions [41,42]. According to previous studies, the optimal loading of ceria promoter should be located at ca. 15 wt% for Ni-based catalysts supported on the mesoporous silica carriers such as SBA-15 and SBA-16 for DRM reaction [31,43]. The enhanced interaction between Ni nanoparticle and ceria over HMS could better improve the dispersion of active Ni species and achieve the high syngas formation rate. Moreover, the optimized ceria content of 15 wt% favors the formation of a high concentration of oxygen vacancy as well as Ce³⁺, serving the in situ coke removal and promoting the carbon resistance [31,37].

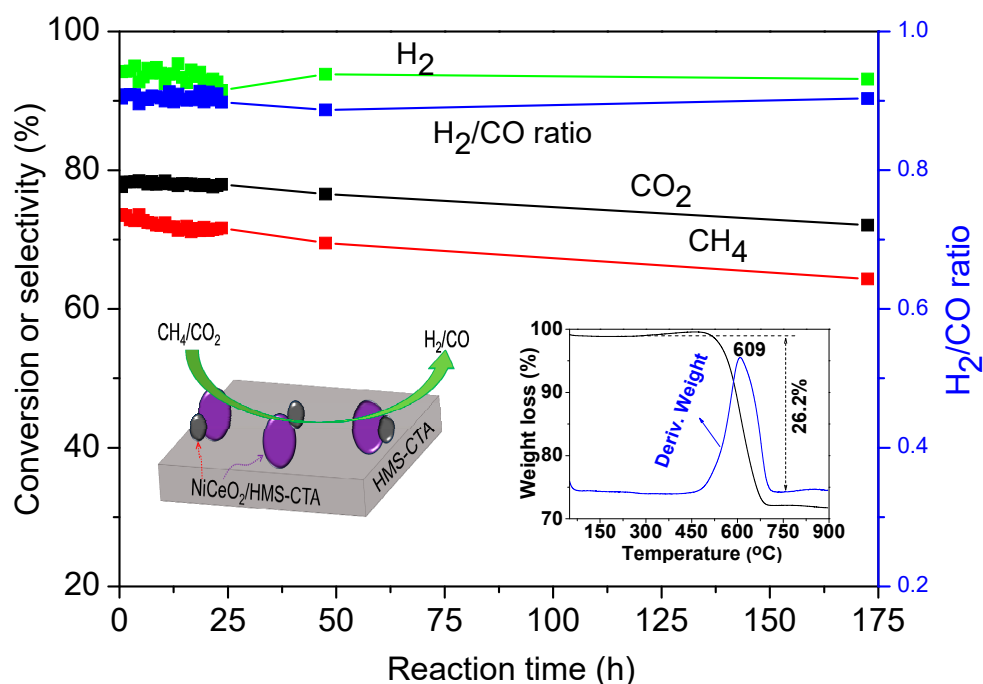


Figure 7. DRM activity results for the 5Ni15CeO₂/HMS-CTA catalyst, the left inserted image stands for the reaction mechanism, the right inserted image presents the weight loss curve of the used catalyst.

3. Materials and Methods

3.1. Materials

All chemicals, including anhydrous citric acid, tetraethyl orthosilicate ($\geq 98\%$, TEOS), poly (ethylene glycol)-block-poly (propylene glycol)-block-poly (ethylene glycol) (P127, $M = 12,600 \text{ g mol}^{-1}$), anhydrous ethanol, cerium (III) nitrate hexahydrate and nickel nitrate hexahydrate were purchased from Sigma-Aldrich (Burlington, MA, USA).

3.2. Materials Preparation

HMS materials were synthesized via a self-assembly strategy in deionized water, using F127 as single template and TEOS as the silica precursor. Typically, TEOS (8.75 g) and a certain amount of citric acid were added to a premixed solution (125 mL water and 2.5 g copolymer template P127) and the mixture was stirred at 38 °C for 24 h. The resulting solution was poured into a Teflon autoclave and hydrothermally synthesized at various temperatures (60 °C, 100 °C or 140 °C) for different time ranges from 4 h to 20 days (Table 1). After that, the crystallized precursor was filtered, washed, and dried at 100 °C for 24 h. Finally, the white powder product was calcined at 550 °C for 6 h to gain hierarchical mesoporous silica.

The above-mentioned HMS materials (2 g) were impregnated with an aqueous solution of Ce(NO₃)₃ (0.073 mol/L) and Ni(NO₃)₂ ($2.5 \times 10^{-4} \text{ mol/L}$), then dried at 100 °C for 12 h. After that, the materials were calcined at 750 °C for 2 h to obtain the catalyst. CeO₂ and Ni loadings were at 15 and 5 wt%, separately, which was labeled as 5NiO15CeO₂/HMS-CTA.

3.3. Catalytic Activity Testing

DRM reaction was investigated in a fixed-bed quartz reactor (ID: 7 mm) at ambient pressure. Specifically, catalysts (150 mg, 45–60 mesh) were uploaded in the center of the quartz reactor tube with the help of quartz wool. Before activity testing, catalysts were pretreated with a flow of 10% H₂/He (50 mL/min) at 700 °C with a heating rate of 5 °C/min for 1 h. Then, the feed gas (CO₂/CH₄/Ar/N₂ = 3:3:3:1) was introduced to the catalyst bed at a total flow rate of 50 mL/min (GHSV of 20,000 mL·g_{cat}⁻¹·h⁻¹). The exhausted products

were studied using online Gas Chromatograph (Agilent GC-6890, Santa Clara, CA, USA) equipped with a TCD detector (a Carbon-Plot coupled with a HP-Plot capillary column).

3.4. Materials Characterization

Small-angle (2θ : $0\text{--}6^\circ$) and normal X-ray diffraction (2θ : $5\text{--}80^\circ$) XRD patterns were measured on a Bruker D8 Advance X-ray diffractometer with a $\text{Cu K}\alpha$ irradiation. N_2 adsorption–desorption isotherms curves were analyzed on a Micromeritics ASAP 2420 automatic analyzer and the temperature of pretreatment was settled at $200\text{ }^\circ\text{C}$ under vacuum for 12 h. A FEI Tecnai G2 F20 Transmission electron microscopy (TEM) was employed to test the pore structure of the HMS synthesized materials. Hydrogen temperature programmed reduction (H_2 -TPR) experiment was carried out to study the reduction properties of $5\text{NiO}15\text{CeO}_2/\text{HMS-CTA}$ catalyst on a chemisorption (Thermo Scientific, Waltham, MA, USA, AutoChemII 2920) instrument. The weight loss curve of the spent $5\text{Ni}15\text{CeO}_2/\text{HSM}$ was obtained on a Thermogravimetric analysis instrument (TGA Q500, New Castle, England).

4. Conclusions

In sum, we advocated an improved, facile one-pot hydrothermal route to prepare hierarchical mesoporous silica (HMS) materials using a single ABA type of non-ionic triblock copolymer structure-directing agent under a novel polycarboxylic acid mediated condition. The process parameters such as citric acid concentration, hydrothermal temperature and crystallization time had been systematically studied. Results revealed that the spatial structure of HMS highly hinges on the concentration interval of citric acid ranges from 0.018 M to 1.82 M owing to the incomplete protonation and bridging effect of citric acid, while the hydrothermal temperature and aging time could more likely impact the pore distribution and size due to the condensation reactions. Moreover, as-synthesized HMS-CTA supported Ni/CeO_2 catalysts displayed a long-term stability of 172 h during the DRM reaction. The improved synthesis route for HMS under citric acid medium exhibits great potential for other hierarchical mesoporous materials synthesis and applications in heterogenous catalysis, environmental governance and nanomedicine and so on.

Author Contributions: Experiment, L.L. and Z.G., writing—original draft, L.L. and J.D., characterization, L.L. and Y.L., writing—review and editing, L.L., J.D. and Y.L., project administration, Y.L. and W.C. All authors have read and agreed to the published version of the manuscript.

Funding: This research receives no external funding.

Acknowledgments: We appreciate the Chinese Scholarship Council (CSC) and Institute of Sustainability for Chemicals, Energy and Environment (ISCE2, A*star, Singapore) for financial support. The authors feel grateful to Yeo Wen Cong and Wang Luo for experimental help, Melissa Prawirasatya for TEM characterization.

Conflicts of Interest: The authors declare no conflict of interest.

References

1. Chang, Y.F.; Li, Y.Z.; Zhang, C.; Zhao, T.Y.; Tuo, X.C.; Guo, J.; Gong, Y.M. Formaldehyde-controlled synthesis of multishelled hollow mesoporous SiO_2 microspheres. *Langmuir* **2019**, *35*, 14517–14521. [[CrossRef](#)] [[PubMed](#)]
2. Wu, L.; Li, Y.; Fu, Z.Y.; Su, B.L. Hierarchically structured porous materials: Synthesis strategies and applications in energy storage. *Natl. Sci. Rev.* **2020**, *7*, 1667–1701. [[CrossRef](#)] [[PubMed](#)]
3. Yang, P.D.; Deng, T.; Zhao, D.Y.; Feng, P.Y.; Pine, D.; Chmelka, B.F.; Whitesides, G.M.; Stucky, G.D. Hierarchically ordered oxides. *Science* **1998**, *282*, 2244–2246. [[CrossRef](#)] [[PubMed](#)]
4. Todorova, S.; Blin, J.L.; Naydenov, A.; Lebeau, B.; Karashanova, D.; Kolev, H.; Gaudin, P.; Velinova, R.; Vidal, L.; Michelin, L.; et al. Co-Mn oxides supported on hierarchical macro-mesoporous silica for CO and VOCs oxidation. *Catal. Today* **2021**, *361*, 94–101. [[CrossRef](#)]
5. Qin, L.M.; Niu, D.C.; Li, N.; Luo, X.F.; Qin, X.; Chen, J.Z.; Li, Y.S.; Shi, J.L. Hydrophobicity-induced electrostatic interfacial self-assembly for porous silica nanospheres with tunable pore sizes and pore hierarchies. *Chem. Eng. J.* **2021**, *405*, 126936. [[CrossRef](#)]

6. Kerkhofs, S.; Willhammar, T.; Noortgate, H.V.D.; Kirschhock, C.E.A.; Breynaert, E.; Tendeloo, G.V.; Bals, S.; Martens, J.A. Self-Assembly of pluronic F127—silica spherical core-shell nanoparticles in cubic close-packed structures. *Chem. Mater.* **2015**, *27*, 5161–5169. [[CrossRef](#)]
7. Zhao, D.Y.; Huo, Q.S.; Feng, J.L.; Chmelka, B.F.; Stucky, G.D. Nonionic triblock and star diblock copolymer and oligomeric surfactant syntheses of highly ordered, hydrothermally stable, mesoporous silica structures. *J. Am. Chem. Soc.* **1998**, *120*, 6024–6036. [[CrossRef](#)]
8. Chen, W.C.; Kuo, S.W.; Chang, F.C. Self-assembly of an A–B diblock copolymer blended with a C homopolymer and a C–D diblock copolymer through hydrogen bonding interaction. *Polymer* **2010**, *51*, 4176–4184. [[CrossRef](#)]
9. Shi, C.X.; Du, G.; Wang, J.G.; Sun, P.C.; Chen, T.H. Polyelectrolyte–surfactant mesomorphous complex templating: A versatile approach for hierarchically porous materials. *Langmuir* **2020**, *36*, 1851–1863. [[CrossRef](#)]
10. Li, J.G.; Lin, R.B.; Kuo, S.W. Phase behavior of hierarchical mesoporous silicas prepared using ABC triblock copolymers as single templates. *RSC Adv.* **2013**, *3*, 17411–17423. [[CrossRef](#)]
11. Mohamed, M.G.; Atayde, E.C., Jr.; Matsagar, B.M.; Na, J.; Yamauchi, Y.; Wu, K.C.W.; Kuo, S.W. Construction hierarchically mesoporous/microporous materials based on block copolymer and covalent organic framework. *J. Taiwan Inst. Chem. Eng.* **2020**, *112*, 180–192. [[CrossRef](#)]
12. Esquena, J.; Nestor, J.; Vilchez, A.; Aramaki, K.; Solans, C. Preparation of mesoporous/macroporous materials in highly concentrated emulsions based on cubic phases by a single-step method. *Langmuir* **2012**, *28*, 12334–12340. [[CrossRef](#)] [[PubMed](#)]
13. Zhao, S.; He, M.; Zhou, Y.M.; Sheng, X.L.; Fu, X.Q.; Zhang, Y.W. Synthesis of micro/mesoporous silica material by dual-template method as a heterogeneous catalyst support for alkylation. *RSC Adv.* **2015**, *5*, 28124–28132. [[CrossRef](#)]
14. Liu, C.C.; Li, J.G.; Kuo, S.W. Co-template method provides hierarchical mesoporous silicas with exceptionally ultra-low refractive indices. *RSC Adv.* **2014**, *4*, 20262–20272. [[CrossRef](#)]
15. Stein, A.; Rudisill, S.G.; Petkovich, N.D. Perspective on the influence of interactions between hard and soft templates and precursors on morphology of hierarchically structured porous materials. *Chem. Mater.* **2013**, *26*, 259–276. [[CrossRef](#)]
16. Zhang, J.Y.; Deng, Y.H.; Wei, J.; Sun, Z.K.; Gu, D.; Bongard, H.; Liu, C.; Wu, H.H.; Tu, B.; Schüth, F.; et al. Design of amphiphilic ABC triblock copolymer for templating synthesis of large-pore ordered mesoporous carbons with tunable pore wall thickness. *Chem. Mater.* **2009**, *21*, 3996–4005. [[CrossRef](#)]
17. Li, J.G.; Lin, R.B.; Kuo, S.W. Hierarchical mesoporous silica fabricated from an ABC triblock terpolymer as a single template. *Macromol. Rapid Comm.* **2012**, *33*, 678–682. [[CrossRef](#)]
18. Li, L.M.; Liu, D.P.; Guo, Z.L.; Liu, Y.; Chu, W. Improved facile synthesis of mesoporous SBA-15-CTA using citric acid under mild conditions. *J. Solid State Chem.* **2020**, *282*, 121079. [[CrossRef](#)]
19. Hunge, Y.M.; Yadav, A.A.; Mathe, V.L. Photocatalytic hydrogen production using TiO₂ nanogranules prepared by hydrothermal route. *Chem. Phys. Lett.* **2019**, *731*, 136582. [[CrossRef](#)]
20. Yadav, A.A.; Hunge, Y.M.; Kang, S.W. Porous nanoplate-like tungsten trioxide/reduced graphene oxide catalyst for sonocatalytic degradation and photocatalytic hydrogen production. *Surf. Interfaces* **2021**, *24*, 101075. [[CrossRef](#)]
21. Yadav, A.A.; Hunge, Y.M.; Kang, S.W. Spongy ball-like copper oxide nanostructure modified by reduced graphene oxide for enhanced photocatalytic hydrogen production. *Mater. Res. Bull.* **2021**, *133*, 111026. [[CrossRef](#)]
22. Hirsch, J.J.; Liu, J.; White, J.J.; Wang, Y. The Role of steps on silver nanoparticles in electrocatalytic oxygen reduction. *Catalysts* **2022**, *12*, 576. [[CrossRef](#)]
23. Glotov, A.; Vutolkina, A.; Pimerzin, A.; Nedolivko, V.; Zasyalov, G.; Stytsenko, V.; Karakhanov, E.; Vinokurov, V. Ruthenium catalysts templated on mesoporous MCM-41 type silica and natural clay nanotubes for hydrogenation of benzene to cyclohexane. *Catalysts* **2020**, *10*, 537. [[CrossRef](#)]
24. Ishaq, H.; Dincer, I.; Crawford, C. A review on hydrogen production and utilization: Challenges and opportunities. *Int. J. Hydrog. Energy* **2022**, *47*, 26238–26264. [[CrossRef](#)]
25. Tang, S.; Xu, Y.S.; Zhang, W.D. Embedding thiophene-amide into g-C₃N₄ skeleton with induction and delocalization effects for high photocatalytic H₂ evolution. *Catalysts* **2022**, *12*, 1043. [[CrossRef](#)]
26. Abdulrasheed, A.; Jalil, A.A.; Gambo, Y.; Ibrahim, M.; Hambali, H.U.; Shahul Hamid, M.Y. A review on catalyst development for dry reforming of methane to syngas: Recent advances. *Renew. Sust. Energ. Rev.* **2019**, *108*, 175–193. [[CrossRef](#)]
27. Ekeoma, B.C.; Yusuf, M.; Johari, K.; Abdullah, B. Mesoporous silica supported Ni-based catalysts for methane dry reforming: A review of recent studies. *Int. J. Hydrog. Energy* **2022**. [[CrossRef](#)]
28. La Parola, V.; Liotta, L.F.; Pantaleo, G.; Testa, M.L.; Venezia, A.M. CO₂ reforming of CH₄ over Ni supported on SiO₂ modified by TiO₂ and ZrO₂: Effect of the support synthesis procedure. *Appl. Catal. A-Gen.* **2022**, *642*, 118704. [[CrossRef](#)]
29. Xie, Z.; Yan, B.; Kattel, S.; Lee, J.H.; Yao, S.; Wu, Q.; Rui, N.; Gomez, E.; Liu, Z.; Xu, W.; et al. Dry reforming of methane over CeO₂-supported Pt-Co catalysts with enhanced activity. *Appl. Catal. B-Environ.* **2018**, *236*, 280–293. [[CrossRef](#)]
30. Xu, Y.; Li, J.; Jiang, F.; Xu, Y.; Liu, B.; Liu, X.H. Insight into the anti-coking ability of NiM/SiO₂ (M=ZrO₂, Ru) catalyst for dry reforming of CH₄ to syngas. *Int. J. Hydrog. Energy* **2022**, *47*, 2268–2278. [[CrossRef](#)]
31. Li, L.M.; Liu, D.P.; Guo, Z.L.; Xi, S.B.; Chu, W.; Liu, Y. Insights into Ni and (Ce)SBA-15-CTA interaction and syngas formation rate. *Mol. Catal.* **2021**, *514*, 111850. [[CrossRef](#)]
32. Qiu, C.T.; Wang, S.; Zuo, J.D.; Zhang, B. Photocatalytic CO₂ reduction coupled with alcohol oxidation over porous carbon nitride. *Catalysts* **2022**, *12*, 672. [[CrossRef](#)]

33. Wang, W.; Wu, C.; Sun, R.; Li, D.; Ru, H.Q. Simple and controllable preparation of SBA-15 microspheres by poly(vinyl alcohol)-assisted P₁₂₃ templating system. *Micropor. Mesopor. Mater.* **2020**, *302*, 110211. [[CrossRef](#)]
34. Guo, W.P.; Su, F.; Zhao, X.S. Ordered mesostructured carbon templated by SBA-16 silica. *Carbon* **2005**, *43*, 2423–2426. [[CrossRef](#)]
35. Liang, J.; Liang, Z.B.; Zou, R.Q.; Zhao, Y.L. Heterogeneous catalysis in zeolites, mesoporous silica, and metal-organic frameworks. *Adv. Mater.* **2017**, *29*, 1701139. [[CrossRef](#)]
36. Du, G.; Song, Y.; Li, N.; Xu, L.J.; Tong, C.; Feng, Y.H.; Chen, T.H.; Xu, J.H. Cage-like hierarchically mesoporous hollow silica microspheres templated by mesomorphous polyelectrolyte-surfactant complexes for noble metal nanoparticles immobilization. *Colloids Surf. A* **2019**, *575*, 129–139. [[CrossRef](#)]
37. Wang, F.G.; Han, K.H.; Yu, W.S.; Zhao, L.; Wang, Y.; Wang, X.J.; Yu, H.; Shi, W.D. Low temperature CO₂ reforming with methane reaction over CeO₂-modified Ni@SiO₂ catalysts. *ACS Appl. Mater. Interfaces* **2020**, *31*, 35022–35034. [[CrossRef](#)]
38. Li, D.; Zeng, L.; Li, X.Y.; Wang, X.; Ma, H.Y.; Assabumrungrat, S.; Gong, J.L. Ceria-promoted Ni-SBA-15 catalysts for ethanol steam reforming with enhanced activity and resistance to deactivation. *Appl. Catal. B-Environ.* **2015**, *176*, 532–541. [[CrossRef](#)]
39. Liang, T.Y.; Low, P.Y.; Lin, Y.S.; Tsai, D.H. Spherical porous nanoclusters of NiO and CeO₂ nanoparticles as catalysts for syngas production. *ACS Appl. Nano Mater.* **2020**, *3*, 9035–9045. [[CrossRef](#)]
40. Guo, Y.; Zou, J.M.; Shi, X.; Rukundo, P.; Wang, Z.J. A Ni-CeO₂-CDC-SiC catalyst with improved coke resistance in CO₂ reforming of methane. *ACS Sustain. Chem. Eng.* **2017**, *5*, 2330–2338. [[CrossRef](#)]
41. Lanre, M.S.; Abasaeed, A.E.; Fakeeha, A.H.; Ibrahim, A.A.; Al-Awadi, A.S.; Jumah, A.B.; Al-Mubaddel, F.S.; Al-Fatesh, A.S. Lanthanum–cerium-modified nickel catalysts for dry reforming of methane. *Catalysts* **2022**, *12*, 715. [[CrossRef](#)]
42. Yan, X.L.; Hu, T.; Liu, P.; Li, S.; Zhao, B.R.; Zhang, Q.; Jiao, W.Y.; Chen, S.; Wang, P.F.; Lu, J.J.; et al. Highly efficient and stable Ni/CeO₂-SiO₂ catalyst for dry reforming of methane; effect of interfacial structure of Ni/CeO₂ on SiO₂. *Appl. Catal. B-Environ.* **2019**, *246*, 221–231. [[CrossRef](#)]
43. Zhang, S.H.; Muratsugu, S.; Ishiguro, N.; Tada, M. Ceria-doped Ni/SBA-16 catalysts for dry reforming of methane. *ACS Catal.* **2013**, *3*, 1855–1864. [[CrossRef](#)]